Indian Journal of Engineering & Materials Sciences
Vol. 27, April 2020, pp. 320-332

Optical, structural and thermal properties of hybrid PVA/$CaAl_2ZrO_6$ nanocomposite films

Hebbur Maheshwarappa Gayitri[a], Murad Al-Gunaid[b,c], Siddaramaiah[b] & Akkanagowda Patel Gnana Prakash [d*]

[a]Department of Electronics and Communication Engineering, Sri Jayachamarajendra College of Engineering, JSS Science and Technology University, Mysore 570006, India

[b]Department of Polymer Science and Technology, Sri Jayachamarajendra College of Engineering, JSS Science and Technology University, Mysore 570006, India

[c]Department of Chemistry, Faculty of Education, Thamar University, Dhamar 13020,Yemen

[d]Department of Studies in Physics, University of Mysore, Manasagangotri, Mysore 570006, India

Received:17 July 2019 ; Accepted: 05 March 2020

This report focuses on fabrication, characterization, and fundamental optical, structural and thermal properties of PVA/calcium aluminum doped zirconate ($CaAl_2ZrO_6$) nanocomposites (NCs) films. The PVA-NCs with different amounts *viz.,* 2, 4, 6 and 8 wt% of calcium aluminum zirconate ($CaAl_2ZrO_6$) have been fabricated using solvent casting technique. The NC films structural and morphology have been investigated by X-ray diffraction, FTIR and scanning electron microscopy. TEM result indicates that the size of nanoparticles (NPs) lies in the range 10-23nm.. Thermal studies have been evaluated by differential scanning calorimetry (DSC). The optical properties of NCs has been investigated by UV-vis spectroscopy, where the optical study reveals an increased refractive index from 1.22 to 2.23 at a wave length of 300 nm, where as the band gap energy (E_g) is reduced from 5.01 to 3.32 eV for PVA to PVA/8wt% $CaAl_2ZrO_6$, respectively. The dielectric studies, optical conductivity measurements and Urbach energy analysis also supports the dopant dependent optical property, tuning of PVA/$CaAl_2ZrO_6$ NC films to enable effective material property engineering to suit specified application requirements.

Keywords: $CaAl_2ZrO_6$, Refractive index, Tauc's plot, Optical conductivity, T_g

1 Introduction

Polymer nanocomposites (NCs) are defined as polymers in which small amounts of nano sized fillers are homogeneously dispersed. The addition of just a few weight percent of the nano sized fillers has profound impact on the physico-mechanical, thermal, opto-electrical and structural characteristics of polymers. This new technology has emerged from the field of engineering and has several applications based on their mechanical, electrical, optical and magnetic properties [1,2]. The outcome of this technology has attracted much attention in view of their application in optical devices. The optical properties are aimed at achieving better reflection, antireflection, interference and polarization properties[3]. These new properties are brought about from the interactions of nanofillers with polymer matrices. The effects of hybrid metal oxide nanosized particle on the optical, structural and thermal properties of PVA matrix are currently of considerable interest[4]. It is recognized that the filling up of the polymer matrix by NPs can enhance the interaction at the polymer filler interfaces. Currently polymeric NCs with good optical clarity and high refractive index have drawn a great deal of scientific interest because of their potential applications in optical filters, waveguides, lenses, light emitting diodes (LEDs) and reflectors. However, optical applications of conventional polymers are limited due to their narrow range refractive indices. Extensive observations have been made by several researchers on the molecular motion and the charge carrier migration in a variety of polar/nonpolar polymers containing one or more fillers[5-6]. Sachin *et al.* [7] investigated the optical properties of PVA/sodium zincate (Na_2ZnO_2) NCs films, for UVA shielding applications. The optical band gap studies reveal a direct band gap relationship with valence band maxima and conduction band minima occurring at same wave vectors. CaO, Al_2O_3 and ZrO_2 are also an important dielectric material that is being investigated

*Corresponding author (E-mail: gnanaprakash@physics.uni-mysore.ac.in)

for potential application as an insulator in transistors in future nano electric devices[8]. Somesh*et al.* [9] have highlighted Photosensitization of optical band gap modified polyvinyl alcohol films with hybrid $AgAlO_2$ nanoparticles its potential to replace SiO_2 in advanced metal oxide semiconductor (MOS) devices and in optical applications. Chandrakala *et al.* [10] investigated structural, electrical and thermal properties of PVA/$LiKZrO_3$ NCs. They observed the electrical conductivity and thermal stability of the NCs increased with increasing NPs content. While, Mallakpour *et al.* [11] investigated morphology, mechanical, thermal and wettability investigations on PVA/ZrO_2 NCs synthesized by aqueous solution-cast technique. The large increase of dielectric relaxation time revealed that the polymers blend matrix produces a large hindrance to the polymer chain dynamics. PVA is a polymer that has been studied intensively because of its excellent film forming ability and these films have high tensile strength, tear and chemical resistance[12]. PVA is one of the promising representatives of polymeric materials and there are numerous applications in electronics, packaging, textile and food packaging due to its easy formability, high clarity, lack of charge density properties and excellent durability[13]. It is thermally stable over a long range of temperature (100– 200 ºC) and below 100 ºC the PVA chains have flexible in nature. Recently, more works of literature investigated and reported on electrical properties of PVA films[14,15]. PVA is a good insulating material with low conductivity and hence, is of importance to the microelectronic industry. PVA is a desirable material for charge storage capacity and dopant-dependent electrical and optical properties. Its electrical and optical conductivity depends on the thermally generated carriers and also with the addition of suitable dopants[16]. The optical applications of conventional polymers are limited due to their narrow range refractive indices. There are numerous reports in literature, which shows an increase in optical conductivity of PVA after incorporation of NPs. Transition metal oxide NPs-loaded polymer-based NC materials are promising candidates which have been constantly developed and investigated to meet newer challenges for opto-electrical applications. One of the most important challenges in the development of NCs is concerned on reducing optical bandwidth, arising refractive index and improving electrical and optical properties which are desirable for opto-electronic applications. The filling up of weak micro-regions of the polymer matrix by NPs may enhance the interaction at the polymer–filler interfaces. Among the above-mentioned NPs, calcium aluminum zirconate NPs have preferred to use strong oxidizing agent of photo generated holes, chemical inertness, non-toxicity, low cost, high refractive index (RI) and good dispersing ability in polymeric system[17,18]. Further, insufficient data in literature is available on the optical thermal and structural properties of PVA/$CaAl_2ZrO_6$ NCs. The main objective in the current investigation is to achieve a deeper consideration of impact $CaAl_2ZrO_6$ NPs to tune the band gap, refractive index, optical conductivity (σ_{opt}), and thermal properties for PVA matrix to enhance PVA NC films for optoelectronic applications.

2 Experimental

2.1 Materials

PVA (average molecular weight 125,000 Aldrich), calcium nitrate [$Ca(NO_3)_2$], aluminum nitrate [$Al(NO_3)_3$] , zirconium nitrate [$Zr(NO_3)_4$,] and glycine [$C_2H_5NO_2$] were purchased from SD fine-chem. Limited, Mumbai, India. Double distilled water was used in this study.

2.2 Synthesis of $CaAl_2ZrO_6$ NPs

In the current investigation calcium, aluminium doped zirconate ($CaAl_2ZrO_6$) NPs have been prepared using sol–gel combustion technique[19]. The appropriate amounts of oxidant nitrates (calcium nitrate ($Ca(NO_3)_2$) , aluminum nitrate ($Al(NO_3)_3$) and zirconium nitrate ($Zr(NO_3)_4$) with molar ratio of Ca: Al: Zr is 0.2: 0.35:0.45 and glycine ($C_2H_5NO_2$) as fuel, were dissolved in double distilled water, separately. The molar ration of fuel to total oxidant nitrates was 2:1. The individual solutions were then mixed together and the pH value was adjusted to 8.5 by adding NaOH solution. Then, the solution was constantly stirred at 90 °C for 2 hrs to obtain dark gel. The gel was continuously heated until the combustion occurred to obtain a fine powder format. Finally, the obtained powder was calcined at 650-800°C for 2 hrs, yields the dark whitish hybrid $CaAl_2ZrO_6$ NPs.

2.3 Fabrication of PVA/$CaAl_2ZrO_6$ NC Films

The 18.75 g of PVA obtained in the powder form was dissolved in 250 ml of double distilled water at 70 °C for about 2 hrs. Then varying amounts viz., 2, 4, 6, and 8 wt% $CaAl_2ZrO_6$ NPs were added to aqueous PVA solution by mechanical stirring followed by ultra sonication for 30 min. The

homogeneous solution was poured into a cleaned glass mold and the solution was allowed to evaporate in the room temperature for 72 hrs to get dry films. Finally, the samples were dried in a hot air oven at 50 °C for 4-5 hrs for complete removal of solvent. The measured thickness of the obtained NC films varied from 0.22 to 0.25 mm. The synthesis and fabrication process of PVA/$CaAl_2ZrO_6$ NC films is as shown in the schematic 1.

2.4 Characterization

The FTIR spectra of the fabricated films were recorded in the ATR mode in the spectral range 4000−400 cm^{-1} using JASCO 4100 spectrometer, Japan, with spectra resolution of 4 cm^{-1}. The morphological behaviors of the PVA/$CaAl_2ZrO_6$ NC films were recorded by a Hitachi 3400, Japan, scanning electron microscope (SEM) coupled with energy dispersive X-ray spectroscopy (EDS).The X-ray powder diffraction (XRD) patterns were recorded using a Bruker diffractometer (Germany) in the scanning range of 10°−70° (λ= 1.54 Å). The optical absorption characteristics of the developed films were established by a Schimadzu-1800 spectrophotometer (Japan) in the spectral range of 220−800 nm. The thermal behaviors of the NCs have been evaluated using differential scanning calorimetry (DSC), TA Q200, USA. Around 6mg of sample was taken and scanned at a heating rate of 10 °C/min in the temperature range 40–240 ºC under nitrogen gas purge. The thermo-analytical testing to determine changes in weight of samples with changes in temperature were carried out using TA instruments, Q600SDT, Australia, The sample was scanned at heated rate of 20 ºC/min under nitrogen atmosphere from ambient temperature to 650 ºC.

3 Results and Discussion

3.1 Morphological and Structural Analysis

The EDS spectrum of Fig. 1(a) shows the atomic % and weight % of the individual elements of NPs and the resulted values are tabulated in Table 1. The tabulated results proved the nano metal oxides containing Ca, Al and Zr with weight percentage in NPs structure.

Furthermore, the presence of inorganic nano ceramics in the organic host was assessed by EDS analysis which distinctly identifies the elemental components of the filler (Ca, Al, and Zr) in the host polymer supporting the possible structural changes in the polymeric host upon filler intercalations. The Morphological features of $CaAl_2ZrO_6$ NPs and pristine PVA and its NCs doped 2, 6 and 8 wt% of $CaAl_2ZrO_6$ NPs were elucidated by SEM and obtained images were displayed in Fig.1 (b–f), respectively.

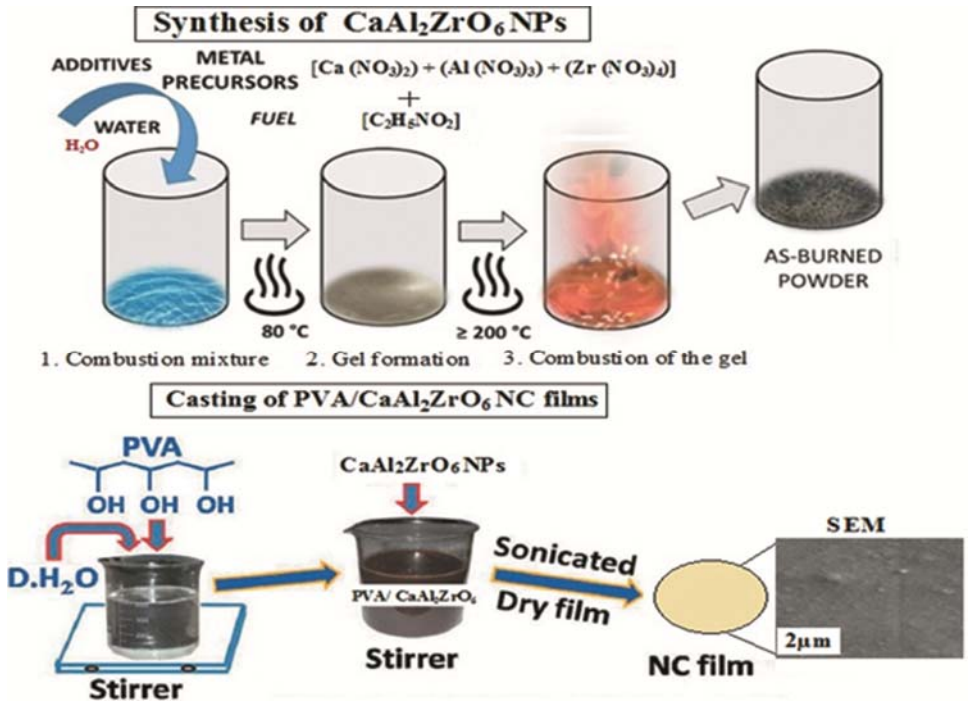

Schematic 1 — Synthesis and fabrication of PVA/$CaAl_2ZrO_6$ NC films.

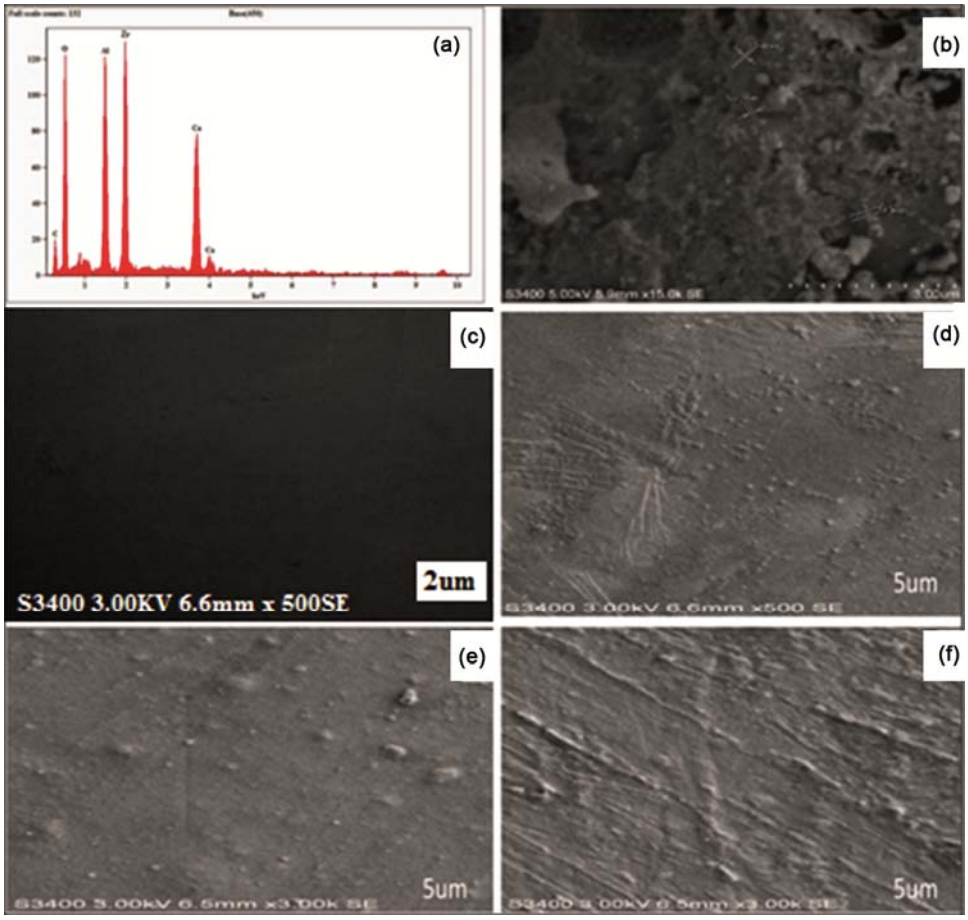

Fig.1 — (a)The EDS spectra of $CaAl_2ZrO_6$ NPs, SEM photomicrographs of (b) $CaAl_2ZrO_6$ NPs, (c) Pure PVA, (d) PVA with 2wt%, (e) PVA with 6wt% and (f) PVA with 8 wt% of $CaAl_2ZrO_6$ NCs.

Table 1 — Quantitative weight and atom percentage of $CaAl_2ZrO_6$ NPs.

Elements	Wt %	Wt % error (±)	Atom %
CK	13.89	0.72	23.39
OK	43.42	0.74	54.90
Al K	13.24	0.23	10.67
Ca K	12.45	0.29	5.78
Ca L	------	------	-----
Zr K	16.99	1.54	5.26
Zr L	-------	------	-----
Total	100.00		100

The SEM micro-photographs report the successful and uniform incorporation of $CaAl_2ZrO_6$ NPs in PVA matrix. The size of the NPs is calculated using XRD graphs and it is found to be 18-25 nm, which is correlated with the TEM results. The increasing NPs content in PVA matrix results the surface rough-ness of the NC films, which could be attributed to the strong physical interactions between NPs and polymer matrix. At a higher filler concentration the distance between NPs becomes closer so the agglomeration of NPs can be noticed.

The XRD experiments have been conducted to examine the micro structural behavior of PVA and its NCs. The XRD profiles of $CaAl_2ZrO_6$ NPs and all NCs are depicted in Fig. 2(a, b) and the estimated parameters are summarized in Table 2. The Scherrer length (L) of PVA/ $CaAl_2ZrO_6$ NCs has been calculated using Scherrer formula[20];

$$L = \frac{K\lambda}{\cos\theta\beta} \quad \ldots(1)$$

where, k is the constant (k = 0.9), which is related to the crystallite shape, λ and θ are the radiation wavelength and Bragg's angle respectively, and β is the full width at half maximum of the diffraction peak. It is note that the average particle size deduced from XRD data was slightly different from that observed from TEM. The XRD pattern of pristine PVA exhibit an intense peak of PVA at $2\theta = 19.9^{o}$ (corresponded to a d spacing of 4.54 Å and reflection

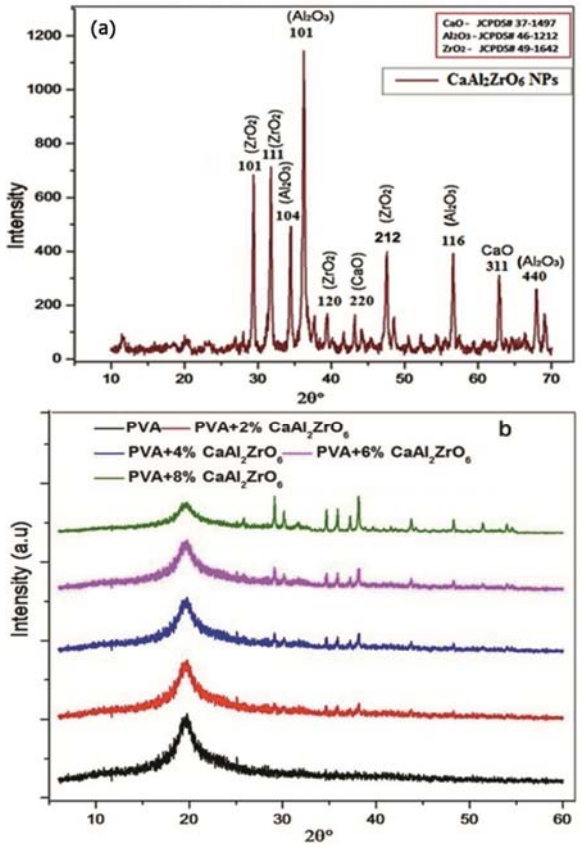

Fig. 2 — XRD patterns for (a) $CaAl_2ZrO_6$ NPs and (b) PVA/$CaAl_2ZrO_6$ NCs.

Table 2 — Structural parameters of PVA/at 2θ =19.9˚.

Composites	β (FWHM), Radian	Scherrer length, L (A˚)	Lattice Strain	η x10^{-3}(A˚)$^{-2}$	SF	R
PVA	0.07	20.1	0.06	2.47	0.07	4.09
$CaAl_2ZrO_6$ *	0.25	5.63	0.24	30.6	0.26	2.91
PVA+2% $CaAl_2ZrO_6$	0.09	14.1	0.10	6.21	0.11	4.26
PVA+ 4% $CaAl_2ZrO_6$	0.11	12.7	0.13	9.81	0.14	4.29
PVA+ 6% $CaAl_2ZrO_6$	0.13	11.2	0.13	10.71	0.13	4.31
PVA+8% $CaAl_2ZrO_6$	0.14	9.59	0.14	11.3	0.15	4.32

*Calculated parameters of pure $CaAl_2ZrO_6$ NPs at corresponding 2θ =36.1°

plane 101), which indicates the semi-crystalline nature of PVA[21]. Furthermore small peaks at 29.3° (101), 31°(111), 34.1° (104), 36.8° (101), 56.63° (212), 47.4 ° (212), 56.6° (116), 62.8° (311), 68°(440), which indicates well crystalline nature of synthesized $CaAl_2ZrO_6$ NPs which is good agreement with JCPDS card numbers, CaO-JCPDS#37-1497, Al_2O_3- JCPDS# 46-1212 and ZrO_2-JCPDS# 49-1642 respectively. It can be noticed from XRD profiles (Fig. 2(a, b) that, a slightly shift of 2θ in the position of the peaks for PVA/NCs as compared to the main peak of pristine PVA. It may be due to the strong intermolecular interaction between PVA and NPs. The Scherrer length (L) of $CaAl_2ZrO_6$ PVA NCs decreased and FWHM values increase with an increase in $CaAl_2ZrO_6$ contents in the PVA matrix. It may be indicated to increasing the amorphous nature of the PVA in NCs. As compared with pure PVA matrix the diffraction peak of NC films with increasing the NPs becomes less intense and broader. This effect may be due to a reduced inter molecular H-bond interaction between chains of PVA and $CaAl_2ZrO_6$ at the interface[22]. This will affect the free volume of the matrix. It is also responsible for variation in changes in inter planar distance (d-spacing) (Table 2). Moreover, the lattice strain (β cos θ/4) and dislocation density ($\eta = 1/L^2$) have been calculated for the peak at 2θ = 19.9° for all NCs. The obtained lattice strain and dislocation density values increases with an increase in the dosage of $CaAl_2ZrO_6$ NPs in NCs due to create defects and morphology of PVA changed lead to increase structural disorder in PVA matrix. Further, the micro-structural parameters such as inter-crystallite separation (R) and stacking fault (SF) were determined using the relations as follows[23]:

$$R=\frac{5\lambda}{8\,sin\theta} \quad \ldots(2)$$

$$SF=\left[\frac{2\pi^2}{45(\tan\theta)^{\frac{1}{2}}}\right]\beta \quad \ldots(3)$$

where, λ is the wavelength of X-ray (1.54056 Å), θ is the diffraction angle, and β is the FWHM of prominent intensity peak. It was noticed from Table 1 that, the variation of R with increased SF values is indicated to the structural interaction of polymer chains with embedded $CaAl_2ZrO_6$ NPs. The trend of R values is consistent with that the values of doped PVA with the data published elsewhere[24].

Transmission Electron Microscope (TEM) and its SAED was experimented in order to investigate the particle size and shape of hybrid $CaAl_2ZrO_6$ NPs shown in Fig. 3 (a, b) respectively.

The TEM micrographs reports the shape and distribution of the NPs with particle size lies in the range 10-23nm. The Fig. 3(b) represents the selected

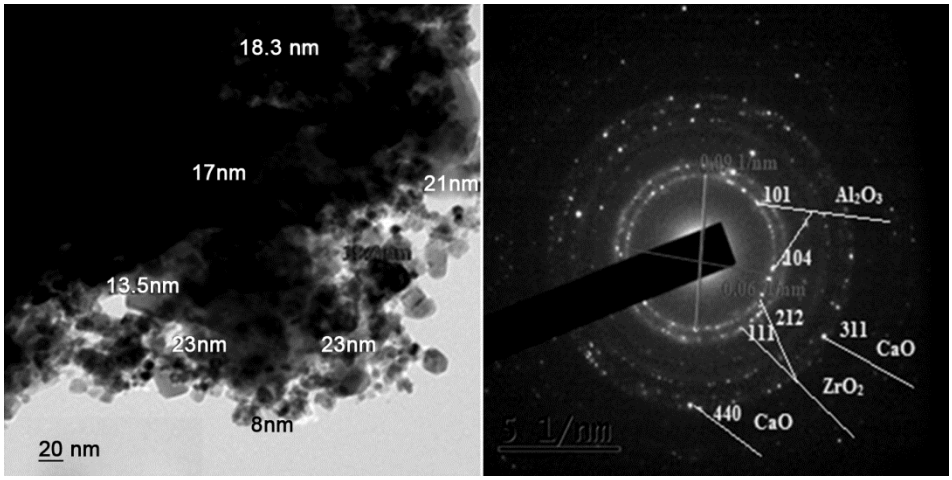

Fig. 3 — (a) TEM micro photographs and (b) SAED pattern of $CaAl_2ZrO_6$ NPs.

area electron diffraction (SAED) pattern evidenced the crystallinity of the formed calcium doped aluminum zirconium PVA NCs.

The FTIR spectra of PVA and its NC films are displayed in Fig.4 (a-e) at wave number range from 4000 - 500 cm^{-1}. FTIR provides information about the effects and interactions between the various constituents in the polymer NCs. The vibration peaks at 3262, 2922, 1728, 1415, 1378, 1250, 1082, 1019 and 835 cm^{-1} are assigned to the signature vibration bands of PVA[25]. The observed strong bands at 3350-3305 cm^{-1} are assigned to -OH stretching vibration of hydroxyl groups of PVA. The band appear at 2922 cm^{-1}corresponding to C-H asymmetric stretching vibration and C-H symmetric stretching vibration at 2855 cm^{-1}. The $CaAl_2ZrO_6$ NPs modified IR bands of PVA in NCs as shown in Fig.4 (a-e). The changes in the stretching vibration of -OH at 3350-3305 cm^{-1} and asymmetric C-H stretching (2918 cm^{-1}) affirm the changes in cross structural behaviors of PVA refer to the effect of $CaAl_2ZrO_6$ NPs in PVA matrix. The decrease in the intensities of -OH stretching vibrations and their relative broadening may be attributed to the physical interaction between the $CaAl_2ZrO_6$ NPs and -OH groups in PVA[26].The intensity of the peak slightly reduced at 1728 cm^{-1} for C=O stretching vibration (refer to residual acetate group) with increasing the $CaAl_2ZrO_6$ NPs dosage. The intensity of the peak at 1082-1008 cm^{-1} of C-O group in PVA is decreases with increase in NPs contents. Furthermore, the peaks at the region 1415–1378 cm^{-1} may be attributed to the bending vibration of C–H in-plane of backbone chains. The characteristic -CH_2 wagging in out-plane is found to be shifted to 835 cm^{-1} and -CH_2 rocking is noticed at

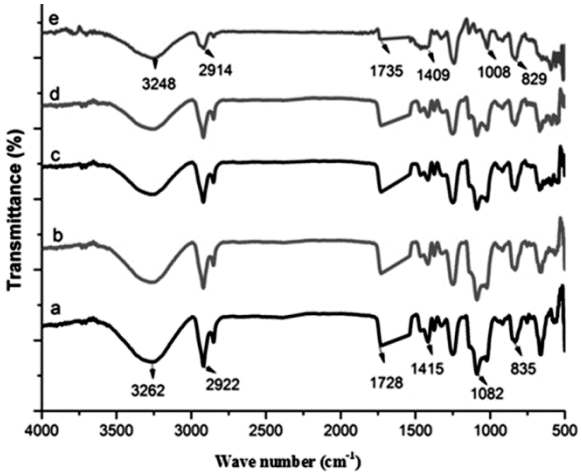

Fig. 4 — FTIR spectra of PVA NCs (a) 0, (b) 2, (c) 4, (d) 6 and (e) 8 wt% of $CaAl_2ZrO_6$ NPs.

around 658 cm^{-1}. Fig. 4(a-e) shows two IR absorption peaks at 552 and 625 cm^{-1}, which clearly indicates the presence of metal oxide NPs in NC films [27].

3.2 Optical Study

The UV–Visible absorbance and transmittance spectra of PVA and its NC films with 2, 4, 6, and 8 wt% of $CaAl_2ZrO_6$ NPs are displayed in Fig. 5(a, b). The absorbance spectra in the region 220-800 nm for PVA NC films is displayed in Fig.5a. The UV–visible spectra of pure PVA exhibited a small absorption peak at 230-250 nm, which may be due to $\pi \rightarrow \pi^*$ electronic transition (k-band) from unsaturated C=O of residual acetate groups present in PVA structure and C=C which exists in the tail head of the polymer. From the spectrum a wide and weak electronic absorption peak in the UV region 260–270 nm with a maximum absorption peak at around 266 nm was noticed. It can be ascribed that to the transition of

unshared electron pair namely (n → π*) of oxygen atoms in PVA structure as a result to absorption of incident light[28].

The optical transmittance spectra of the $CaAl_2ZrO_6$ NC films as function of wavelength in the range 220- 800 nm are shown in Fig. 5(b) as can be seen in the visible wavelength region the films are transparent and the transparency of the $CaAl_2ZrO_6$ films reduces and reaches 27% by increasing the wavelength and increasing filler concentration. The interference fringes can be absorbed in the transmittance spectra indicating that the films have a uniform thickness and homogeneous[29].

The modeling and design of optically functional materials is escort by an important criterion termed optical energy gap (E_{opt}). The optical band gap energy can be obtained from the optical absorption spectrum using the following relationship:

$$\alpha h\nu = C[h\nu - E_g]^{r} \quad \ldots(4)$$

where, C is a constant, E_g is the optical band gap of the material and the exponent r depends on the nature of electronic transition. The r is an index which is assumed to have values of 1/2, 3/2, 2 and 3, depending on the nature of electronic transition. If r picks up a value of 1/2, the nature of transition is direct allowed transition; whereas r with a value of 2 implies indirect allowed transition. In order to determine the band gap direct and indirect transition the plots $(\alpha h\nu)^{2}$ and $(\alpha h\nu)^{1/2}$ as a function of energy ($h\nu$) is plotted in Fig.6 (a, b).

The plots of $(\alpha h\nu)^{1/2}$ as a function of photon energy ($h\nu$) yields a straight line. The extrapolation of linear portions of these curves gives the values of optical band gaps for the NCs. The variation of optical band gap of PVA NCs with varying amounts of NPs content is displayed in Fig.6(a, b) and the calculated values of band gap for both direct and indirect band transitions are summarized in Table 3. As can be seen

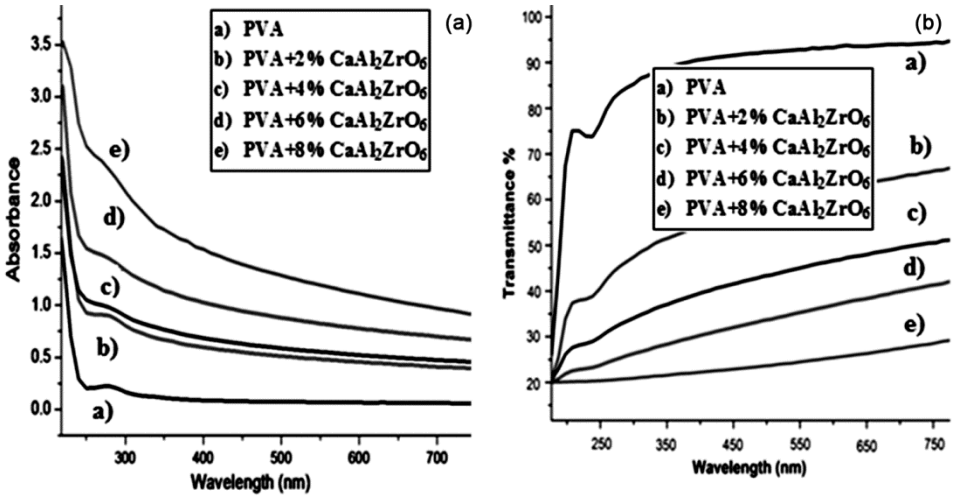

Fig. 5 — (a) Absorbance (b) Transmittance spectra of PVA/$CaAl_2ZrO_6$ NCs as a function of wavelength.

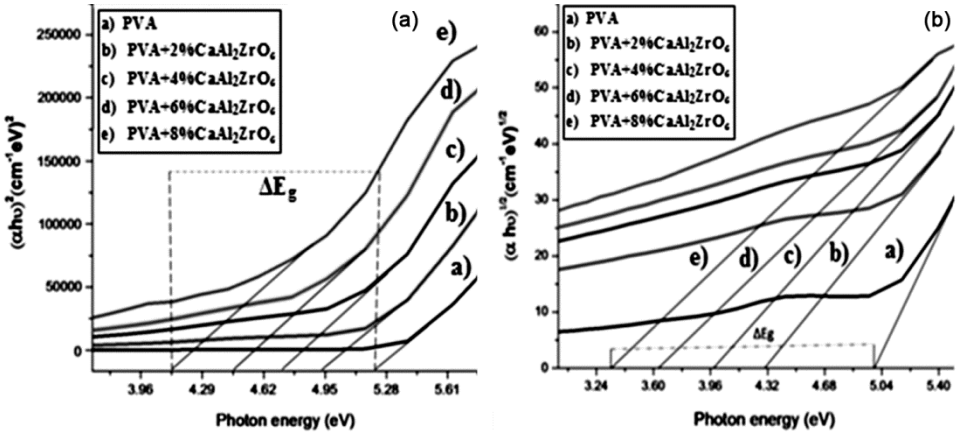

Fig. 6 — Tauc's plot of (a) Direct and (b) Indirect band gap energy diagrams of PVA/$CaAl_2ZrO_6$ NCs.

from Fig. 6(a) the value of optical energy gap for un doped PVA film is around 5.01 eV, indicating that the material is an insulator. However, introduction of NPs resulted in a gradual decrease in band gap energies from 5.01eV to 3.37eV, with an increase in doping ($CaAl_2ZrO_6$) levels from 0 to 8wt %. The observed variation in band gap energies with increasing dopant content may be due to the formation of charge transfer complexes between $CaAl_2ZrO_6$ NPs and −OH groups of PVA, as supported by FTIR analysis[30]. The interaction of NPs with PVA may also lead to the formation of new molecular dipoles originating from structural defects induced after doping[31]. The increase in the concentration of $CaAl_2ZrO_6$ NPs in PVA increases the number of molecular dipoles; these dipoles create localized sites between the valence and conduction energy bands, making lower energy transitions feasible. These band gap tunable materials are suitable for optoelectronic applications.

The optical conductivity of PVA/$CaAl_2ZrO_6$ NCs (Fig. 7(a)) was determined using the following relation;

$$\sigma = \frac{\alpha n c}{4\pi} \quad \ldots (5)$$

where, c is the velocity of light, α is the absorption coefficient and n is the refractive index. The variation of optical conductivity as a function of wave length is shown in Fig. 7(a). It is seen that an increase in NPs content increases the conductivity of the NC films, and it is found that the maximum conductivity of 2.89×10^{12} S^{-1} is achieved for PVA/8 wt % of $CaAl_2ZrO_6$ NCs. The observed behavior may be due to a molecular ordering effect by activated electronic states either by thermally or electrically with an increase in conducting filler content[32].

The application of polymers in the field of optics and optoelectronics is often restricted owing to their relatively lower range of refractive indices. However, in recent years it has been overcome by addition of inorganic fillers with a wide range of *n* can result in polymeric composites with extreme refractive index, thereby increasing the application window of the resultant materials in the field of optoelectronics[33], and the effect is found to be maximum with inorganic nanosized fillers due to their lesser density and higher surface area. Thus, in the current investigation, the effect of $CaAl_2ZrO_6$ NPs addition on the refractive index (n) of the PVA films were studied and the variation is presented as a function of wavelengths in Fig. 7(b) and the corresponding *n* values are tabulated in Table 3. The obtained results indicate an increase in n values of PVA NC films with an increase in filler content. The increase in *n* of the composite may be attributed to the increased density of the films with an increase in filler content, which, in turn, owed to a continuous increase in the number of atomic refractions due to increase of the linear polarization. This enhanced packing density of polymer composites with NPs inclusions may lead to the formation of strong intermolecular bonding between the introduced NPS and the −OH groups of PVA through electrostatic interactions.

The dependence of the extinction coefficient on the wavelength in the range 200-800 nm of pure PVA and

Table 3 — Optical parameters of $CaAl_2ZrO_6$ NCs.

wt% of $CaAl_2ZrO_6$ in PVA	*n* at $\lambda_{300\ nm}$ ± 0.04	$E_{g.dir}$ (eV)	$E_{g.ind}$ (eV)	σ_{opt} (s^{-1}) x 10^{12}	K	E_u (eV)
0	1.22	5.04	5.14	1.2	0.004	1.26
2	1.31	4.03	4.83	2.1	0.007	1.45
4	1. 42	3.98	4.72	2.5	0.009	1.59
6	1.58	3.68	4.42	2.7	0.010	1.97
8	2.23	3.32	4.14	3.2	0.011	2.28

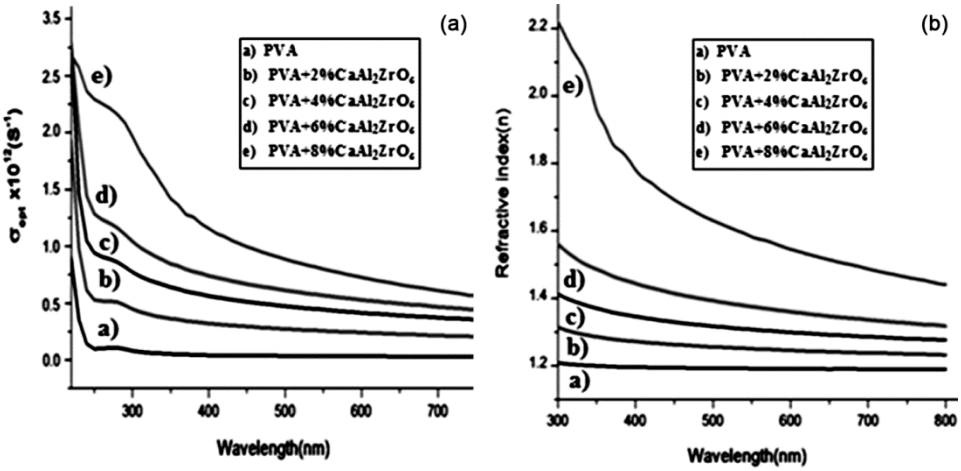

Fig. 7 — (a) Optical conductivity (b) Refractive index of PVA/$CaAl_2ZrO_6$ NCs.

doped samples is shown in Fig. 8 (a). The obtained values of extinction coefficient (K) are summarized in Table 3. It is clear that the extinction coefficient for pure PVA sample shows a decrease in values of the wavelength from 200-800 nm, while it increases extinction coefficient after doping the samples (2, 4, 6 and 8%), in the wavelength from 300 to 800 nm. The extinction coefficient was increased for NCs with increasing doping concentration; this is due to the increase in absorption coefficient, where the extinction coefficient depends on the absorption coefficient by the following equation[34,35]:

$$K=\frac{\alpha\lambda}{4\pi} \quad \ldots (6)$$

where, α is the absorption coefficient.

The absorption coefficient near the fundamental absorption edge is exponentially dependent on photon energy (hν) and obeys the empirical Urbach relation. The Urbach energy (E_U), which is the width of the tails states in the band gap associated with the structural defects and disorder within the polymer matrix, can be calculated by the relation[36],

$$\alpha(h\nu) = \alpha_0 \exp\left(\frac{h\nu - E_1}{E_U}\right), \; h\nu < E_g, \quad \ldots (7)$$

where $\alpha(h\nu)$ is the absorption coefficient as a function of the photon energy ($h\nu$) and α_o and E_1 are constants determined from $ln(\alpha)$ versus $h\nu$ plot (Fig. 8(b)). E_1 approximately coincides with the energy of the lowest free exciton state at zero temperature. The value of E_U was obtained from the inverse of the slope of $ln\alpha$ versus $h\nu$, and the obtained values are listed in Table 3. The E_U values change inversely with optical band gap[37]. E_U is often interpreted as the width of the tail of localized states in the gap region associated with the tailing of the valance band density of states and is broader than the conduction band tail.

The Wemple-DiDomenico model is used to describe the dielectric response for transitions below the optical gap to calculate the single-oscillator parameters. The dispersion data of the refractive index can be described by a single-oscillator model, where E_0 and E_d are single-oscillator constants[38];

$$n^2 - 1 = \frac{E_o E_d}{{E_o}^2 - (h\nu)^2} \quad \ldots (8)$$

E_0 is the single-oscillator energy and E_d is the dispersion energy which measures the average strength of inter band optical transition. The values of E_0 and E_d can be obtained from the intercept (E_0/E_d) and slope ($-1/E_0E_d$) of the linear fitted lines from the plots $1/(n^2-1)$ versus $(h\nu)^2$ as shown in Fig. 9(a), E_0 is empirically related to the lowest optical band gap as; $E_0 = 1.5\, E_g$ [39].

The optical behavior of materials is described by optical constants. Fig. 9(b) shows the absorption coefficient spectra of pure PVA and PVA/$CaAl_2ZrO_6$ NC films. It is obvious that the absorption coefficient increases with increasing $CaAl_2ZrO_6$ NPs concentration in PVA/$CaAl_2ZrO_6$ NCs. As is known, PVA is transparent in the visible region. This is clearly shown in Fig. 5(b), the transmittance gradually decreases in the PVA/$CaAl_2ZrO_6$ NCs sample. The formula absorbance coefficient (α = absorbance/films thickness) was used to calculate the dependence of the absorption coefficient (α) on frequency.

The calculation of real part and imaginary part of the dielectric constant provide information about the loss factor. Fig. 10 (a, b) shows the variation of real and imaginary parts of dielectric constants ($\varepsilon_r = n^2 - k^2$

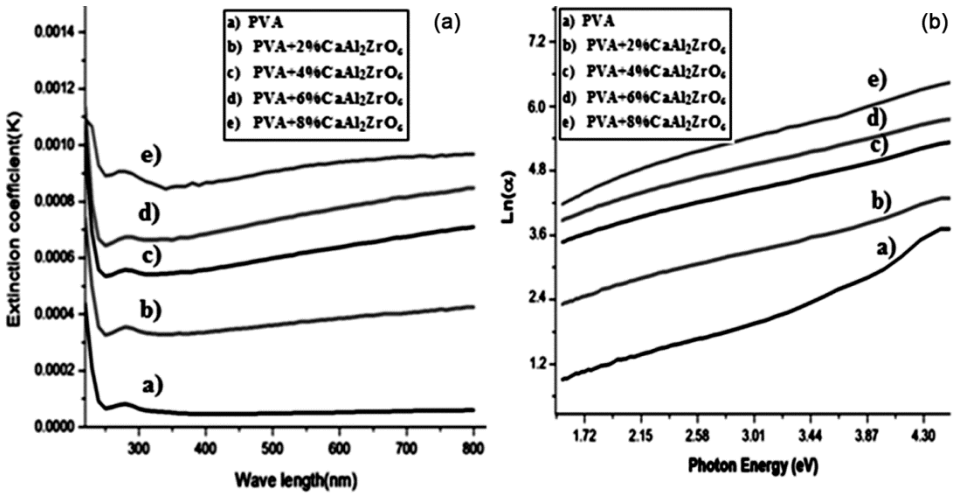

Fig. 8 — (a) Extinction coefficient (b) Urbach plot (ln(α)) of PVA/ $CaAl_2ZrO_6$ NCs.

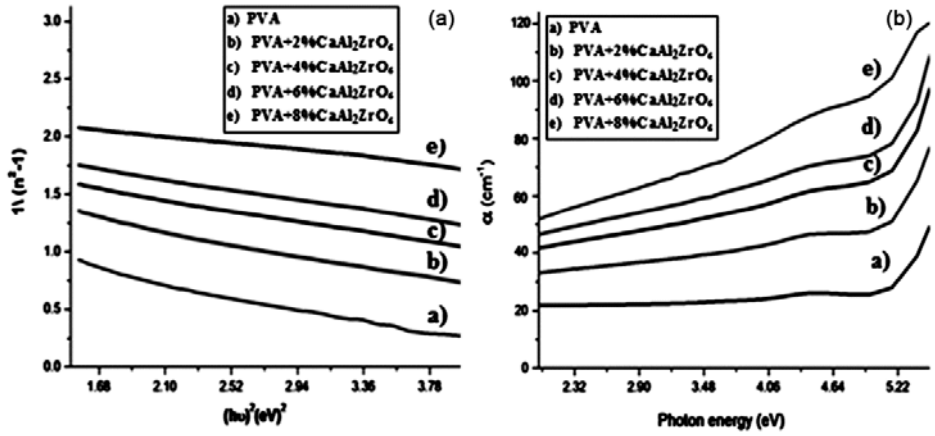

Fig. 9 — Plot of (a) $(n^2-1)^{-1}$ versus $(h\upsilon)^2$ and (b) Absorption coefficient (α) of PVA/$CaAl_2ZrO_6$ NCs.

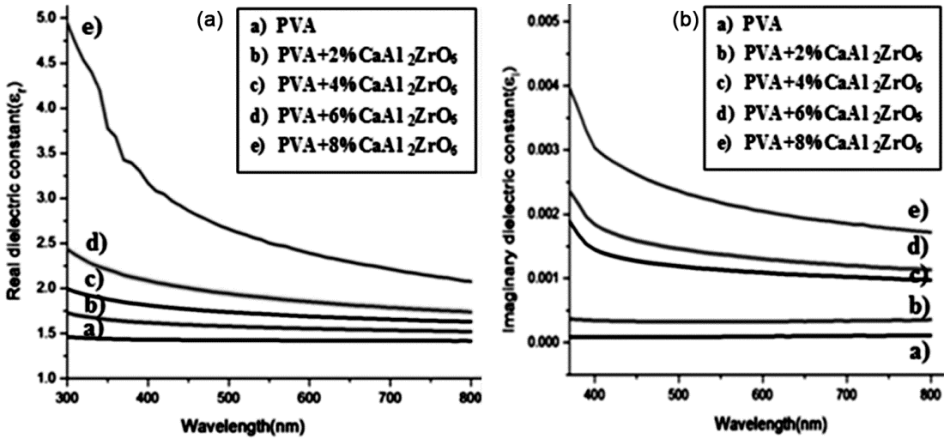

Fig. 10 — Plot of (a) Real dielectric and (b) Imaginary dielectric constant of PVA/$CaAl_2ZrO_6$ NCs.

and $\varepsilon_i=2nk$) of composites. It is concluded that the variation of ε_r mainly depends on (n^2) because of small values of (k^2), while ε_i mainly depends on the (k) values which are related to the changes of absorption coefficients[40]. The real part of the dielectric constant is associated ability of the material to slow down the speed of light. Imaginary part shows absorption energy of dielectric material to from an electric field due to dipole motion[41].

3.3 Thermal Properties

The effect of $CaAl_2ZrO_6$ content on thermal properties of PVA/$CaAl_2ZrO_6$ films were studied by DSC to probe the effect of $CaAl_2ZrO_6$ contents on the glass transition temperature (T_g), melting temperature (T_m), the heat of fusion (ΔH_m) and percent of crystallinity on PVA. DSC thermograms of pure PVA and its NC films as a function of temperature is depicting in Fig. 11.

The obtained thermal parameters for PVA/$CaAl_2ZrO_6$ are summarized in Table 4. Figure 11 reveals that the pure PVA has Tm at around 191°C, which is in good agreement with the reported data elsewhere[42]. It may be attributed to strong hydrogen bonds were expected to effects on the mobility of PVA chains. The incorporation of $CaAl_2ZrO_6$ NPs into PVA matrix shows shift of T_m, T_g and heat of fusion (ΔH_m) peaks towards lesser temperature, 188 °C, 62 °C and 18.6 for PVA/8wt% $CaAl_2ZrO_6$ NC, respectively. It may be due to the crystalline portion of the PVA structure was influenced by the addition of NPs.

A similar kind of observation for T_m was reported elsewhere[43]. The reduction in T_m for NCs may be due to strong interactions between free electrons of oxygen (–OH groups of PVA) and empty orbital of NPs by charge transfer complex (CTC) formation. Moreover, a significant reduction in T_g from 72°C to 62 °C with an increase in NPs content from 0 to

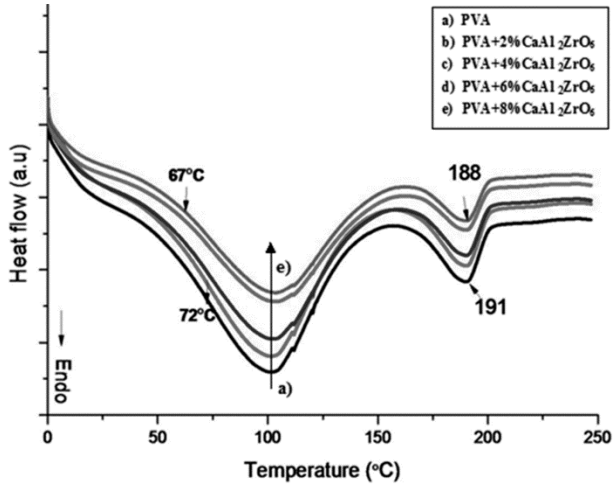

Fig. 11 — DSC thermograms of pure PVA and PVA/$CaAl_2ZrO_6$ NCs.

Table 4 — Data obtained from DSC thermo grams for PVA/$CaAl_2ZrO_6$ NCs.

$CaAl_2ZrO_6$ in PVA (wt%)	T_g (ºC)	T_m(ºC)	ΔH_m(J/g)	Crystallinity (%)
0	72	191	27.2	19.3
2	70	190	24.4	17.6
4	68	189	22.3	15.5
6	64	189	20.2	13.7
8	62	188	18.6	13.2

8 wt% indicates that shortage of hydrogen bonds between PVA chains due to the new interaction occurred between the components in NCs.

The percent of crystallinity (χ_c) for all NCs, and semi crystalline PVA have been calculated from the relation;

$$\chi_c = \frac{\Delta H_m}{\Delta H_0} \text{x} 100 \quad \ldots (9)$$

where, ΔH_m is the melting enthalpy (from DSC curve) and ΔH_0 is enthalpy of 100% crystalline PVA (138.6 J/g)[44].

The obtained result shows χ_c was decreasing with an increase in the $CaAl_2ZrO_6$ dosage in NCs. The decrease in χ_c as a function of NPs content described to the mutual influences between the components in NCs. The result reveal that the enthalpy of fusion (ΔH) as well as percentage of crystallinity (χ_c) of PVA NCs decreases with increasing filler in NCs films indicating amorphous domains formed in NCs.

The thermo gravimetric (TG) profiles of PVA and its $CaAl_2ZrO_6$ NPs reinforced composite films are represented in Fig. 12. The percentage of thermally induced weight loss and their corresponding temperatures are tabulated in Table 5.

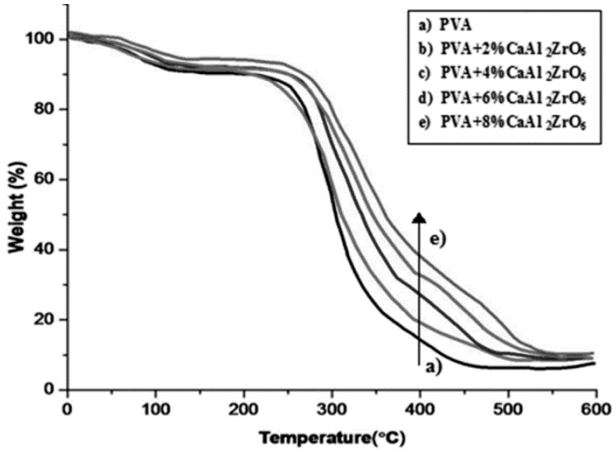

Fig. 12 — TG curves of PVA/$CaAl_2ZrO_6$ NCs.

Table 5 — Thermal data obtained from the TGA profiles of PVA/ $CaAl_2ZrO_6$ NC films.

$CaAl_2ZrO_6$ in PVA (wt%)	Degradation stages	Temperature ± 1.5 (°C)		Weight Loss (%)
		T_o	T_f	
0.0	1	54	107	8
	2	232	362	67
	3	360	474	17
	Ash	-	-	8
2.0	1	62	114	7
	2	256	352	53
	3	372	495	28
	Ash	-	-	12
4.0	1	63	116	8
	2	257	353	55
	3	369	496	25
	Ash	-	-	14
6.0	1	64	112	6
	2	257	358	52
	3	367	497	25
	Ash	-	-	17
8.0	1	65	113	6
	2	257	359	54
	3	360	502	22
	Ash	-	-	18

All samples (PVA and PVA/$CaAl_2ZrO_6$ NC) under study undergo a three step thermal decomposition. The first step weight loss region in the temperature range (T_0 - T_f) 54 to 107^{0}C corresponds to removal of physically adsorbed water molecules[45]. The dependence of thermally induced weight loss of PVA NCs on $CaAl_2ZrO_6$ NP content, summarized in Table 5, ascertains a decrease in weight loss with increasing metal oxide NPs loadings. The observed changes in weight loss is associated with decreased

mobility of polymer chains, owing to possible chelation of $CaAl_2ZrO_6$ nanostructures with PVA, in agreement with the data reported elsewhere[46]. The major weight loss appearing at the second stage involved thermal decomposition (224-378 °C), while the third and final weight loss is due to backbone fragmentation and/or chain-scission (360-486 °C)[47].

The introduction of $CaAl_2ZrO_6$ nanostructures (thermal insulation barriers) induced a shift in decomposition temperatures of PVA to higher temperatures with increasing the filler loadings. The observed increase in decomposition temperatures ascertain increased thermal stability of PVA with $CaAl_2ZrO_6$ loadings, which in-turn supports a possible physical interaction between –OH groups of PVA with $CaAl_2ZrO_6$ NPs, well-in agreement with X-ray diffraction studies.

4 Conclusion

The PVA/$CaAl_2ZrO_6$ NCs with varying amounts of NPs were prepared by solvent intercalation technique. The effect of different amounts of $CaAl_2ZrO_6$ NPs on the structural, optical and thermal properties of the NCs has been studied. The FTIR analysis showed a positive interaction between PVA matrix and $CaAl_2ZrO_6$ NPs. XRD profile results show the structural reordering takes place with reduction in the crystallinity. The TEM image indicates the uniform size and shape of NPs. A significant improvement in refractive index of PVA/$CaAl_2ZrO_6$ NCs at higher dosage 8wt% NPs as compared to reported values in literature for higher dosage of NPs by retaining its optical transparency. The increasing $CaAl_2ZrO_6$ NPs bridge the gap separating localized states in energy level of PVA caused to enhance optical electrical conductivity. The optical conductivity, RI and dielectric constants of PVA/$CaAl_2ZrO_6$ NCs increase with an increase in the dosage of $CaAl_2ZrO_6$ NPs. DSC results indicate the reduction in Tg of NC films.The DSC and thermo gravimetric measurements substantiate excellent thermal stabilities. Additionally the flexibility of PVA/$CaAl_2ZrO_6$ films coupled with enhanced optical parameters may enable these NCs explored for their potential uses in optical displacement devices.

References

1 El-Shamy A G & Zayied H S S, *Synt Met*, 259 (2020) 116218.

2 Ramazanov M A, Hajiyeva F V, Babayev Y A, Valadova G V, Nuriyeva S G & Shirinova H A, *J Elast Plasti*, 52 (2020) 159.

3 Bi D, Li Y, Yao Y, Tao T, Liang B & Lu S, *J Alloys Compounds*, 825 (2020) 153998.

4 Heiba Z K & Mohamed M B, *Opt Quantum Electro*, 52 (2020) 99.

5 Zhou L & Jiang Y, *Mater Sci Technol*, 36 (2020) 1.

6 Heiba Z K & Mohamed M B, *J Molecu Struct*, 1181 (2019) 507.

7 Shivanna S, Subramani N K, Swamy K, Nagaraj S K, Muthuraj J R B & Siddaramaiah *J Luminescence*, 208 (2019) 494.

8 Alhazime A A, Mohamed M B & Abdel-Kader M H, *J Inorganic Organometall Polym Mater*, 29 (2019) 436.

9 Somesh T E, Al-Gunaid M Q & Madhukar B S, *J Mater Sci: Mater Electro*, 30 (2019) 49.

10 Chandrakala H N, Ramaraj B & Siddaramaiah, *J Phys Chem Solids*, 75 (2014) 252.

11 Mallakpour S. and Shafiee E. *Ultrasonics Sonochemistry*, *40 (*2018) 889.

12 Jebur Q M, Hashim A & Habeeb M A, *Trans Electrical Electronic Mater*, 20(2019) 334.

13 Chebil A, Doudou B B, Dridi C & Dammak M, *Mater Sci Eng: B*, 243 (2019) 125.

14 Patel M H. Chaudhuri T K, Patel V K, Shripathi T, Deshpande U & Lalla N P, *RSC Adv.* 7 (2017) 4422.

15 Shivanna S, Subramani N K, Swamy K, Nagaraj S K, Muthuraj J R B & Siddaramaiah, *J Luminescence*, 208 (2019) 488.

16 Suma G R, Subramani N K, Shilpa K N, Sachidananda S & Satyanarayana SV, *J Mater Sci: Mater Electron*, 28 (2017) 10707.

17 Gaaz T, Sulong A, Akhtar M, Kadhum A, Mohamad A, Al-Amiery A, *Molecules*, *20* (2015) 22833.

18 Hemalatha K S & Rukmani K, *RSC Advances*, 78 (2016) 74354.

19 Ji W Q, Zhang Q H, Wang C F & Chen S, *Industr Eng Chem Res*, 55 (2016) 11705.

20 Freeda M & Subash T D, *Mater Today Proc*., 4 (2017) 4301.

21 Anandraj J & Joshi G M, *J Inorg Organomet Polym Mater*, 27 (2017) 1850.

22 Chandrakala H N, Ramaraj B, Shivakumaraiah & Siddaramaiah, *J Alloys Compounds,* 586 (2014) 333

23 Gayitri H M Murad Q A, Madhukar B S, Siddaramaiah & Gnana Prakash A P, *Polym-Plast Technol Eng*, 58 (2019) 1124

24 El Sayed A M, El-Gamal S, Morsi W M & Mohammed G J, *Mater Sci*, 50 (2015) 4717.

25 Gayitri H M, Murad Al-Gunaid, Siddaramaiah & Gnana Prakash A P, *Polymer Bulletin,* https://doi.org /10.1007/s00289-019-03069-3

26 Kundu P P, Biswas J, Kim H & Choe S, *Eur Polym J,* 39 (2003) 1585.

27 AL-Gunaid M Q A, Saeed A M N, Subramani N, Madukar B S & Siddaramaiah, *J Mater Sci Mater Electron,* 28 (2017) 8086.

28 Praveena S D, Ravindrachary V, Bhajantri R F & Ismayil, *Polymer Comp*, 37 (2016) 997.

29 Murad QA , Adel M N, Gayitri H M & Siddaramaiah, *Polym-Plast Technol Eng*, 59 (2020) 483.

30 Siddaiah T, Ojha P, Kumar NO & Ramu **C**, *Mater Res*, 21 (2018) 5.

31 Kojima Y, Usuki A, Kawasumi M, Okada A, Fukushima Y, Kurauchi T T & Kamigaito, J. Polym. Sci., Part A*: Polym Chem*, 31(1993) 983.

32 Al-Gunaid M Q A, Saeed A M N & Siddaramaiah*, J Appl Polym Sci,* 135(2018) 45852.

33 Tomita Y, Aoi T, Oshima J & Odoi K, *Adv Modern Trends VI*, 11030 (2019) 1103007,

34 Shivanna S. Subramani N K, Swamy K, Nagaraj S K, Muthuraj & Siddaramaiah, *J Luminescence*, 208 (2019) 494.

35 Nangia R, Shukla N K & Sharma A, *J Molecular Struct*, 1177 (2019) 330.

36 Jebur Q M, Hashim A & Habeeb M A, *Trans Electrical Electronic Mater*, 21 (2020) 48.

37 Ahmed H, Abduljalil H M & Hashim A, *Trans Electrical Electronic Mater*, 20 (2019) 232.

38 Kadham A J, Hassan D, Mohammad N & Ah-yasari A H, *Bulletin Electrical Eng Inform*, 7 (2018) 34.

39 Bdewi S F, Abdullah O G, Aziz B K & Mutar A A R, *J Inorg Organomet Polym Mater,* 26 (2016) 326.

40 Dan H, Gu Tan J, Zhang B & Zhang Q, *Progress Organic Coat*, 120 (2018) 259.

41 James J, Unni A B, Taleb K, Chapel J P, Kalarikkal N, Varghese S, Vignaud G & Grohens Y, *Nano-Structures Nano-Objects,* 17 (2019) 42.

42 Kobayashi, Manabu H, Saito B, Boury K, Matsukawa & Sugahara Y, *Appl Organometall Chem*, 27 (2013) 677.

43 Howell I R, Colella C, Li N S, Ito K & Watkins J J, *ACS Appl Mater Interfaces*, 7 (2015) 3646.

44 Volonakis G, Sakai N, Snaith H J & Giustino, *J Phys Chem Lett*, 10 (2019) 1728.

45 Wageh S, Al-Ghamdi A A, Al-Turki Y, Tjong S C, El-Tantawy F & Yakuphanoglu F, *J Nanoelectronics Optoelectronics*, 11 (2016) 440.

46 Hassan D & Hashim A, *Bulletin Electrical Eng Inform*, 7 (2018) 551,

47 Aziz S B, Ahmed H M, Hussein A M, Fathulla A B, Wsw R M & Hussein R T, *J Mater Sci: Mater Electron*, 26 (2015) 8028.